Advances in vascular biology: imaging of abdominal organs and skin development

Stripling, K.

Chapter 6

Epidermis-specific *Atp6ap2* Deletion Impairs Development and Maintenance of the Skin - ATP6AP2 Controls Skin Morphogenesis and Homeostasis

Martin S, Stripling K*, Nguyen T*, Ramos V, Thalgott JH, Aractingi S, Koster J, Rabelink TJ, Raymond K#, Lebrin F#

** Contributed equally* *# Contributed equally*

Abstract

The prorenin receptor (PRR), also known as ATP6AP2, is a multifunctional transmembrane protein situated on Xp11.4 chromosome in human. PRR regulates blood pressure through the reninangiotensin system (RAS), establishes pH homeostasis via its interaction with the vacuolar-proton ATPase (V-ATPase), and mediates Wnt signaling during neurogenesis. However, the role of PRR is still largely unknown in skin development and homeostasis. To study the effect of ATP6AP2 in skin, we generated a mouse model with epidermis-specific deletion of *Atp6ap2*. *Atp6ap2* deletion provoked embryonic lethality due to hemorrhages formation at around E15.5. RNA-Seq analysis of skin samples at E15.5 provided evidence that protein homeostasis, processing, and maturation are dysregulated indicating keratinocyte stress. At postnatal stage, inducible epidermis-specific deletion of *Atp6ap2* caused chronic inflammation associated with epidermal hyperplasia, dermal infiltration of immune cells, as well as an enlargement of lymphatic vessels and lymph nodes. Our data indicate that the absence of ATP6AP2 causes keratinocyte stress, release of interleukin 33 (IL-33), and dermal infiltration of immune cells leading to chronic inflammation that resemble atopic dermatitis. In conclusion, ATP6AP2 plays a central role in embryonic development and postnatal homeostasis of the skin.

Keywords

ATP6AP2 • Keratinocytes • Development • Homeostasis • Inflammation

Introduction

The prorenin receptor (PRR) is a single-transmembrane receptor encoded by the gene *ATP6AP2* (OMIM 300556) situated on Xp11.4 chromosome in human. Although PRR was initially characterized as part of the tissue renin-angiotensin system (RAS), it is now becoming clear that ATP6AP2 is a multifunctional protein. ATP6AP2 not only regulates blood pressure through RAS, but is also involved in controlling the pH homeostasis of cellular organelles via its interaction with the vacuolar-proton ATPase (V-ATPase), thereby interfering with protein clearance [1–3]. Additionally, ATP6AP2 mediates signaling pathways such as Wnt, Notch, and mTOR, requiring acidification for activation [4–7].

ATP6AP2 is a type I transmembrane protein, which is cleaved by the Golgi apparatus into an N terminal fragment (NTF) and C terminal fragment (CTF). NTF is secreted into the cytosol, whereas CTF remains associated with the V-ATPase harboring an endoplasmic reticulum (ER) retrieval motif [8]. Yet, the relative contribution of the different molecular forms of ATP6AP2 (full-length, NTF and CTF) and their functions in different tissues are still largely unknown. Recent studies using conditional *Atp6ap2*-knockout mice have addressed its function in various tissues. Deletion of PRR in kidney epithelial cells, cardiomyocytes, smooth muscle cells, hepatocytes, and neurons were associated with tissue defects causing abnormal organ development and/or maintenance due to impaired V-ATPase function [9–18].

Human genetic analyses revealed two types of mutations in *ATP6AP2*, associated with different disorders. Patients with exon skipping mutations showed neurological disability ranging from X-linked Parkinsonism and epilepsy to fulminant early postnatal neurodegeneration, depending on the percentage of the short transcript [15–18]. Hemizygous missense mutations in the extracellular domain of *ATP6AP2* were responsible for a glycosylation disorder with hepatosteatosis, immunodeficiency, cutis laxa, and psychomotor impairment [19, 20]. These disorders are largely reminiscent in patients deficient for the V-ATPase assembly factors, particularly ATP6AP1 [21]. Although both exon skipping and missense mutations affect ATP6AP2 levels, the ability of ATP6AP2 to bind to ATP6AP1 is impaired suggesting that ATP6AP2 is required for V-ATPase assembly in these tissues. Impaired V-ATPase function leads to a reduced lysosome acidification, which translates into different consequences depending on the tissue susceptibility to protein degradation blockage and acidification-associated signaling pathways.

We have previously reported that ATP6AP2 is expressed in the adult epidermis [22]. To gain insight into its potential role in the skin, we generated mice with epidermis-specific deletion of *Atp6ap2*. Surprisingly, while skin barrier function is required only after birth, our analysis reveals that epidermal ATP6AP2 is essential for embryonic development. We present evidence that beside a strong effect on epidermal development, epidermic loss of *Atp6ap2* causes changes in the cellularity of the dermis including the aberrant formation of veno-lymphatic shunts leading to embryonic lethality at around E15.5.

RNA-Seq analysis of skin samples collected at E15.5 and *in vitro* experiments using *Atp6ap2* deficient keratinocytes collectively suggest that impaired protein clearance in *Atp6ap2*-deficient keratinocytes lead to keratinocyte damage associated with up-regulation of interleukin 33 (IL-33), which recruits various immune cells to respond to this stress. This local enrichment of immune cells may trigger the formation of veno-lymphatic shunts in the developing skin.

These data indicate that epidermal ATP6AP2 plays an essential role in the maintenance of dermal-blood lymphatic separation during skin development. To study the role of ATP6AP2 in postnatal epidermis, we used a mouse model in which epidermis-specific deletion of *Atp6ap2* can be induced by Tamoxifen injection. We demonstrate that postnatal *Atp6ap2* deletion in the epidermis led to a chronic inflammation associated with epidermal hyperplasia, dermal infiltration of immune cells, and enlargement of lymphatic vessels and lymph nodes, pinpointing to a skin disorder that resembles atopic dermatitis.

Results and Discussion

We previously reported that ATP6AP2 is expressed in the basal cell layer of the interfollicular epidermis (IFE) and hair follicle (HF) in adult skin [22]. Immunofluoresence analysis revealed that epidermal expression of ATP6AP2 was detectable from E13.5 and was maintained along development till adulthood, selectively in the basal cell layer of the epidermis (**Figure 1A**, **S1A**). To investigate the role of ATP6AP2 in the skin, female mice harboring floxed *Atp6ap2* alleles (*Atp6ap2* $^{F/F}$) were crossed with transgenic males expressing Cre recombinase under control of the Keratin 5-promoter (*K5-Cre*) active in the basal epithelial cells [23] (**Figure S1B**). Since *Atp6ap2* is situated on the X chromosome, litters were *K5-Cre*; *Atp6ap2* $^{F/Y}$ knockout males (hereafter referred to as KO; $y/\Delta m$); *K5-Cre*; *Atp6ap2* $^{F/+}$ heterozygous females (hereafter referred to as HET; $x/\Delta m$), and *Atp6ap2* $^{F/Y}$ and *Atp6ap2* $^{F/+}$ which were used as controls (*Atp6ap2* ^{wt}). Immunofluorescence analysis confirmed efficient deletion of *Atp6ap2* from most basal epithelial cells of KO mice while HET females exhibited mosaic pattern of ATP6AP2-expressing and -deficient basal cells, in line with the random inactivation of either X chromosomes in females (**Figure 1B**, **S1C**).

Although skin barrier function is only necessary after birth, surprisingly, none of the KO or HET mice were found alive at P0. At E18.5 the percentage of living animals was still low at only 7% and 15% for KO and HET mice, respectively. Analysis at E15.5 revealed that embryonic lethality was already at 77% and 79% for KO and HET mice, respectively and strikingly, haemorrhages were observed in the dermis (**Figure 1C**-**D**, **S1D**-**E**). Immunofluorescent staining of whole-mount skin with anti-CD31 and anti-VEGFR3 antibodies to visualize the blood and lymphatic networks respectively, did not uncover major developmental defects in KO and HET mouse skin at E15.5 (**Figure 1E**). Yet, local lymphatic dilation was observed, as well as occasional the presence of CD31/VEGFR3 double positive structures

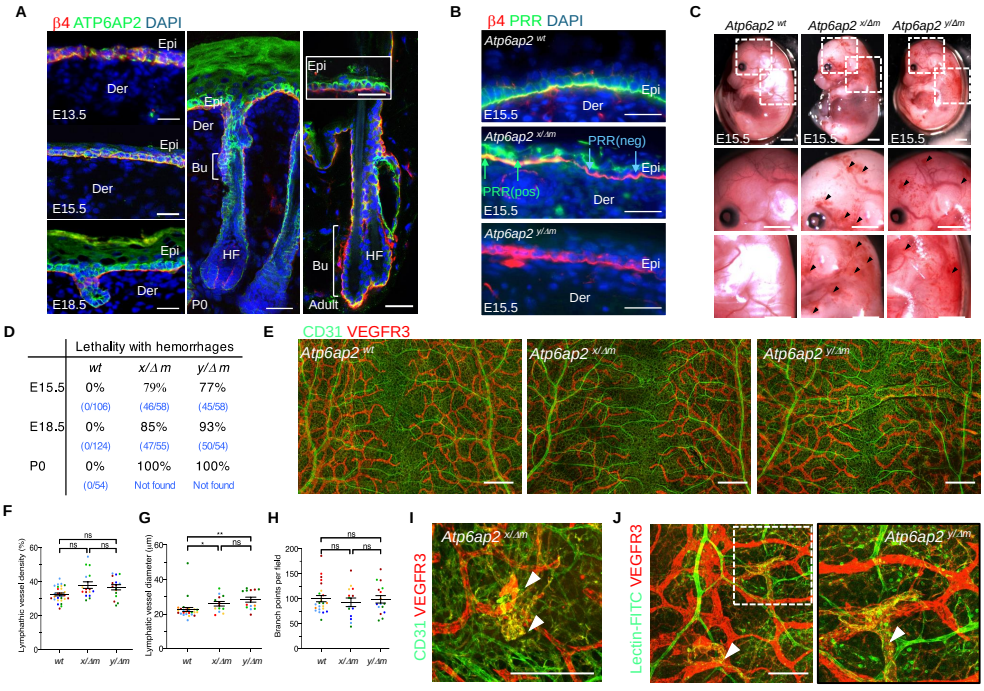

Figure 1 | Reduced ATP6AP2 expression in the epidermis leads to the formation of veno-lymphatic shunts and to embryonic lethality at E15.5. (**A**) Immunofluorescence labelling of sections through back skin isolated from control mice at different stages of embryonic development, with anti-β4 subunit integrin and anti-ATP6AP2 antibodies. Scale bar: 30 µm. (**B**) Immunofluorescence labelling of back skin sections isolated from control, HET, and KO mice at E15.5, with anti-β4 subunit integrin and anti-ATP6AP2 antibodies. Scale bar: 30 µm. (**C**) Photographs of control, HET and KO embryos at E15.5. Arrowheads (►) point to dermal hemorrhages. Scale bar: 1 mm. (**D**) Table showing the percentage of embryonic lethality associated with hemorrhages at E15.5 (n = 27 litters, 106 control, 58 HET and 58 KO embryos), E18.5 (n = 30 litters, 124 control, 55 HET, and 54 KO embryos), and P0 (n = 10 litters, 54 control). (**E**) Whole-mount labeling of control, HET, and KO back skin with anti-CD31 and anti-VEGFR3 antibodies at E15.5. Scale bar: 50 µm. (**F**) Quantitative analysis of the lymphatic vessel density in control, HET, and KO back skin at E15.5. (**G**) Quantitative analysis of the lymphatic vessel diameter in control, HET, and KO back skin at E15.5. (**H**) Quantitative analysis of the lymphatic vessel branch points in control, HET, and KO back skin at E15.5. (**I**) Whole-mount labeling of back skin with anti-CD31 and anti-VEGFR3 antibodies illustrating local co-localization in HET at E15.5 (►). Scale bar: 100 µm. (**J**) Whole-mount labeling with anti-VEGFR3 antibody after injection of Lectin-FITC in the vitellin vein of KO at E15.5. Scale bar: 100 µm.

(**Figure 1F-I**, **S1F**). Injection of Tomato Lectin-FITC in the vitellin vein of KO embryo at E15.5 followed by immunofluorescent staining of whole-mount skin with anti-VEGFR3 antibody displayed the presence of Lectin in VEGFR3 positive vessels, indicating the appearance of venous lymphatic shunts suggesting a blood-filled lymphatic phenotype in KO and HET mice (**Figure 1J**). Together, these observations indicate that ATP6AP2 plays an essential role in the maintenance of dermal-blood lymphatic separation during skin development.

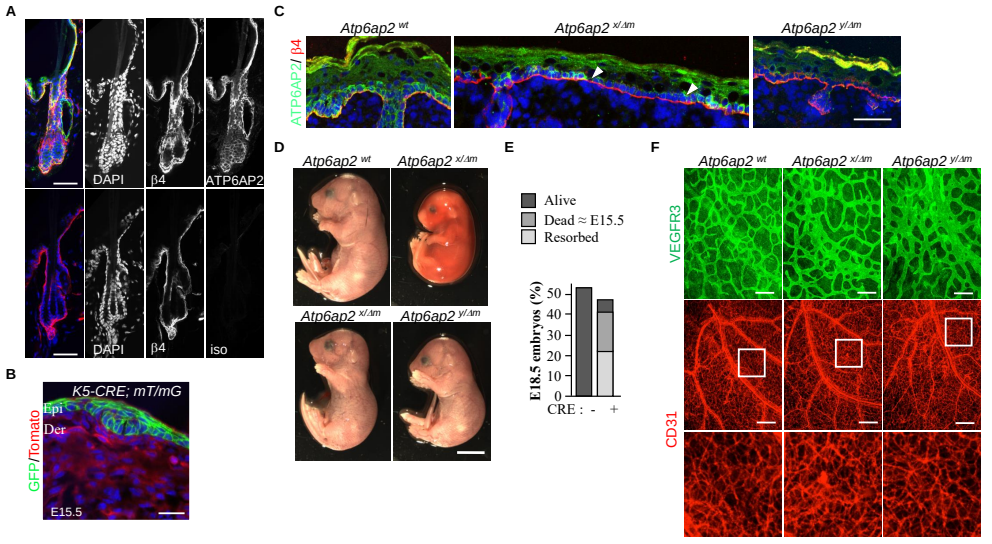

Figure S1 | (**A**) Immunofluorescence labelling of consecutive sections through back skin isolated from adult control mice with anti-β4 subunit integrin and anti-ATP6AP2 (upper panel) or isogenic control (lower panels) to control for anti-ATP6AP2 antibody specificity. Scale bar: 50 µm. (**B**) Lineage-tracing experiment confirms that K5-expressing cells (membrane-bound GFP cells; mGFP) are restricted to basal keratinocytes in skin sections of embryos at E15.5. Scale bar: 20 µm. (**C**) Immunofluorescence labelling of sections through back skin isolated from control, HET, and KO mice at 18.5, with anti-β4 subunit integrin and anti-ATP6AP2 antibodies. Scale bar: 50 µm. (**D**) Photographs of control, HET, and KO E18.5 embryos. Upper panel shows an example of dead HET while lower panels illustrate mutant embryo that survived till E18.5. Scale bar: 5 mm. (**E**) Quantitative analysis of the percentage of alive, dead, and resorbed embryos at E18.5 (n = 30, 236 embryos) at E18.5. (**F**) Whole-mount labeling of control, HET, and KO back skin with anti-CD31 and anti-VEGFR3 antibodies at E15.5. Scale bar: 200 µm.

By investigating the proliferation of basal epidermis cells before embryonic death, a reduced BrdU incorporation rate was encountered with median values of 27.84% and 26.64% for KO and HET compared to 40.12% for control litter mates (**Figure 2A-B**). This was associated with a delay in the shift from predominantly symmetric to asymmetric divisions, which triggers stratification at E14.5, with 55.5 ± 2.2% and 52.8 ± 2.1% of asymmetric divisions observed for KO and HET compared to 70.7 ± 1.3% for control litter mates (**Figure 2C-D**). Furthermore, at this stage no apoptotic cells were virtually detected with the anticleaved caspase 3 antibody in neither control nor mutant skin (not shown). Together, these features led to a reduced thickness in basal proliferative and supra-basal differentiating layers of the epidermis in alive KO and HET embryos at E18.5 (**Figure S2A-F**). All things considered, these data indicate that altered ATP6AP2 abundance affects epidermal progenitor cell activity during skin development.

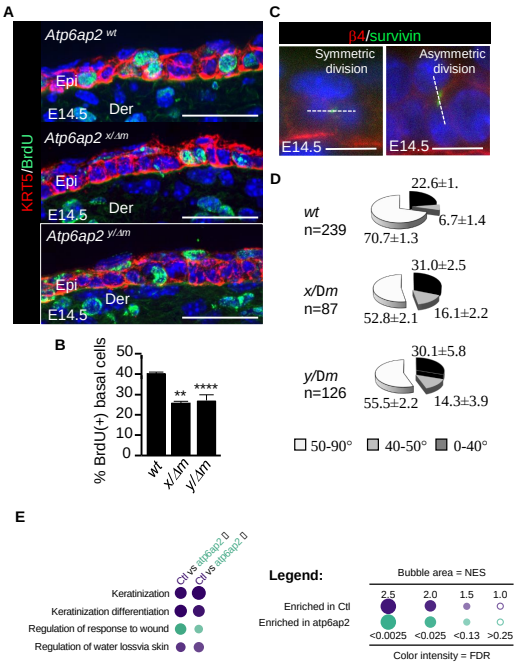

Figure 2 | Reduced ATP6AP2 expression affects epidermis development. (**A**) Immunofluorescence labeling of back skin sections from embryos at E14.5 with anti-BrdU and anti-keratin 5 (KRT5) antibodies. Scale bar: 50 µm. (**B**) Quantitative analysis of the percentage of BrdU-positive (BrdU+) basal cells in skin sections from embryos E14.5 (controls, $n = 9$; Het, $n = 3$; KO, $n = 5$; mean ± SEM; **: $P = 0.0091$, ****: $P \leq 0.0001$, Mann-Whitney). (**C**) Immunofluorescence labeling of back skin sections from embryos at E14.5 with anti-survivin and anti-β4 subunit integrin antibodies illustrating symmetric and asymmetric divisions. Scale bar: 10 µm. (**D**) Quantitative analysis of the proportion of symmetric and asymmetric divisions observed in back skin sections from embryos at E14.5. (**E**) Functional enrichment analysis of pathways associated with epidermal development in back skin at E15.5.

To define the molecular mechanisms controlling skin development by ATP6AP2, we used RNA-Seq to compare the back skin of KO, HET, and control embryos at E15.5. To capture the chronological events, we collected back skin samples from severely affected KO prior to death, poorly affected HET, and their control litter mates. Consistent with a delay in epidermal development, functional enrichment analysis revealed an underrepresentation of pathways involved in skin differentiation and keratinization in KO and HET compared to control embryos at E15.5 (**Figure 2E**). Since these effects were similar in KO and HET mice, an early event was suggested. Quantitative RT-PCR analysis supported these results, confirming the downregulation of basal and supra-basal epidermal markers in KO and HET compared to control back skin at E15.5 (**Figure S2G**).

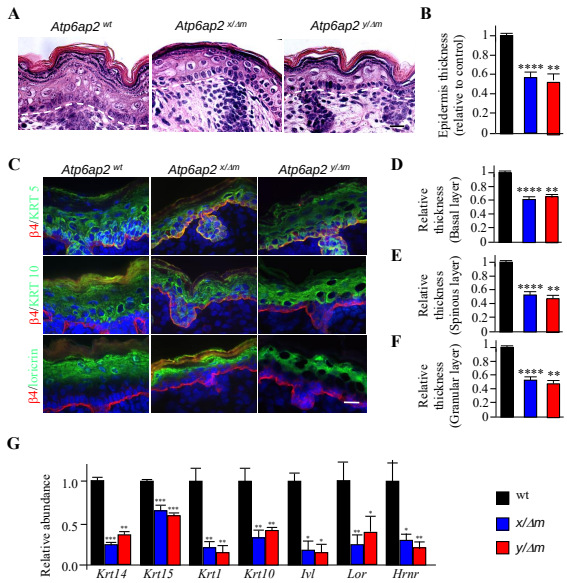

Figure S2 | (**A**) Hematoxylin and Eosin (H&E) staining of back skin sections from surviving embryos at E18.5. Scale bar: 50 µm. (**B**) Quantitative analysis of the epidermis thickness measured after H&E staining of back skin sections from surviving embryos at E18.5. (**C**) Immunofluorescence labeling of back skin sections from surviving embryos at E18.5 with antibodies against β4 subunit integrin and against markers of different layers of the epidermis, i.e., Keratin 5 (KRT5), Keratin 10 (KRT10), and Loricrin. Scale bar: 50 µm. (**D**) Quantitative analysis of the thickness of the basal epidermis layer based on Keratin 5 labelling of back skin sections from surviving embryos at E18.5. (**E**) Quantitative analysis of the thickness of the spinous epidermis layer based on Keratin 10 labelling of back skin sections from surviving embryos at E18.5. (**F**) Quantitative analysis of the thickness of the granular epidermis layer based on Loricrin labelling of back skin sections from surviving embryos at E18.5. (**G**) Quantitative RT-PCR analysis of different markers of the different layers of the epidermis, measured in skin extract of control, HET, and KO embryos at E15.5.

Interestingly, pathways associated with angiogenesis were found to be enriched only in strongly affected KO, indicating the presence of a secondary effect which, on contrary, is not yet visible in less affected HET (**Figure 3A**). Notably, an opposite pattern was present in the mitochondria associated pathway, indicating that only severely affected KO exhibited an energy deficit (**Figure 3B**). Moreover, in line with a defect in protein homeostasis, pathways associated with ER to Golgi transport, protein processing and maturation, proteasome complex, and ribosome biogenesis were underrepresented in KO and HET dorsal skin with similar effects, suggesting that this is an early event (**Figure 3C**). This was accompanied by an immune response, indicated by pathways associated with chemoattractant activity, i.e., leucocytes and monocytes, platelet degranulation, and cytokine activity, i.e., TNF-α and IL-10 being enriched in KO and HET compared to control embryos (**Figure 3D**). A few additional interleukin-associated pathways were specifically enriched in strongly affected KO skin, suggesting more advanced signals.

A total of 1883 and 1298 genes were found to be differentially expressed in KO and HET groups, respectively compared to controls. Notably, there were 88 common differentially expressed genes shared between KO and HET groups. Among them, IL-33 a cytokine known for its significant role in immune and inflammatory responses in the skin acting as an alarmin cytokine released in response to cellular stress, was found to be 2.67 and 2.39-fold upregulated in KO and HET, respectively. To define whether IL-33 production was directly attributable to keratinocytes, we used a keratinocyte cell line carrying a conditional allele of *Atp6ap2* (*Atp6ap2* $^{F/Y}$) established in our laboratory (**Figure S3A-B**). These cells express basal keratinocyte markers, including Keratin 5, Keratin 14, as well integrin α6 β4 (**Figure S3C-D**). The adenoviral delivery of Cre recombinase was optimized to achieve efficient deletion of *ATP6AP2* compared to cells where adenoviral delivery of LacZ was performed (**Figure 3E-F**). Interestingly, this was associated with a reduced EdU incorporation rate, as well as with an upregulation of IL-33, consistent with what was found in KO and HET back skin samples (**Figure 3G-I**). Together, these data suggest that altered ATP6AP2 abundance leads to a defect in protein homeostasis associated with cellular stress. This in turn triggers the release of IL-33 by the keratinocytes, which may serve as an attractant for immune cells. Such events could potentially lead to the local formation of veno-lymphatic shunts, ultimately resulting in embryonic lethality around E15.5.

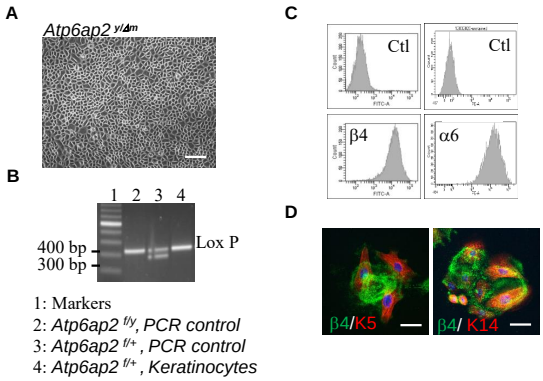

Figure S 3 | (**A**) Micrograph of normal mouse keratinocyte bearing *Atp6ap2* floxed allele (NMK-*Atp6ap2* $^{Flox/Y}$). (**B**) PCR analysis of the loxP site. (**C**) Flow cytometry analysis of NMK-*Atp6ap2* $^{Flox/Y}$ cells with antibodies against β4 and α6 integrin subunits. (**D**) Immunofluorescence labeling of NMK-*Atp6ap2* $^{Flox/Y}$ cells with antibodies against β4 subunit integrin, Keratin 5 (K5), or Keratin 14 (K14).

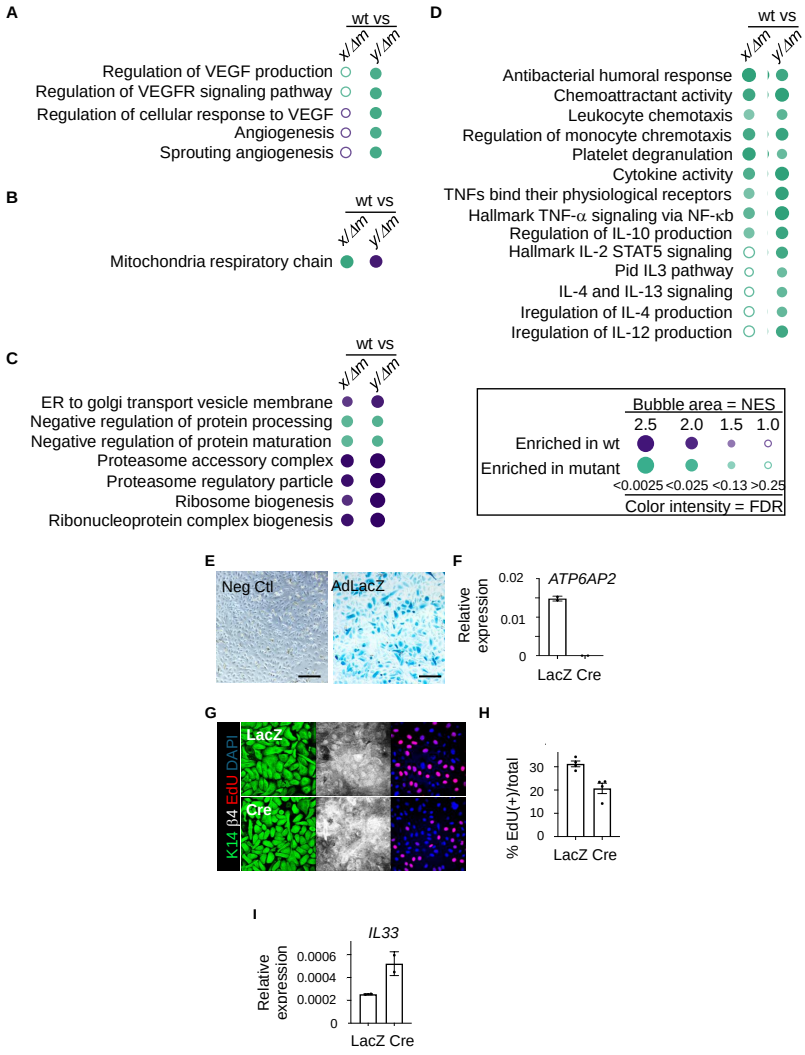

Figure 3 | Molecular mechanisms controlling skin development by ATP6AP2. (**A**) Functional enrichment analysis of pathways associated with angiogenesis in back skin of E15.5. (**B**) Functional enrichment analysis of pathways associated with the mitochondria respiratory chain in back skin of E15.5. (**C**) Functional enrichment analysis of pathways associated with protein homeostasis in back skin of E15.5. (**D**) Functional enrichment analysis of pathways associated with immune response in back skin of E15.5. (**E**) Micrograph of normal mouse keratinocyte bearing *Atp6ap2* floxed allele (NMK-*Atp6ap2* $^{Flox/Y}$) infected (right panel) or not (left panel) with Adenovirus encoding LacZ (MOI 100). LacZ activity is observed after incubation with IPTG. Scale bar: 200 µm. (**F**) Quantitative RT-PCR analysis of *Atp6ap2* relative to *Gapdh* in NMK-*Atp6ap2* $^{Flox/Y}$ infected with Adenovirus encoding LacZ or Cre recombinase (MOI 100). (**G**) Immunofluorescence labelling of NMK-*Atp6ap2* $^{Flox/Y}$ keratinocytes infected with Adenovirus encoding LacZ or Cre recombinase with antibodies against Keratin 14 (K14), β4 subunit integrin, and EdU. Scale bar: 250 µm. (**H**) Quantitative analysis of EdU(+) in NMK-*Atp6ap2* $^{Flox/Y}$ keratinocytes infected with Adenovirus encoding LacZ or Cre recombinase. (**I**) Quantitative RT-PCR analysis of *IL33* relative to *Gapdh* in NMK-*Atp6ap2* $^{Flox/Y}$ infected with Adenovirus encoding LacZ or Cre recombinase.

To study the role of ATP6AP2 in postnatal skin, at a time point when the skin barrier has already been established and the vascular network is in a quiescent state, female mice harboring floxed *Atp6ap2* alleles (*Atp6ap2* $^{F/F}$) were crossed with transgenic males expressing Cre recombinase under control of inducible Keratin 14-promoter (*K14-Cre*^{ERT2}), active in the basal epithelial cells after induction [24]. Litters were injected with Tamoxifen and *K14-Cre*^{ERT2}; *Atp6ap2* $^{F/Y}$ knockout males (hereafter referred to as KO; $y/\Delta m$) and *K14-Cre*^{ERT2}; *Atp6ap2* $^{F/+}$ heterozygous females (hereafter referred to as HET; $x/\Delta m$) were compared to *Atp6ap2* $^{F/Y}$ and *Atp6ap2* $^{F/+}$ litter mates used as controls (*Atp6ap2* ^{wt}).

The postnatal deletion of *Atp6ap2* led to the development of scaly scales in the less hairy regions of the skin, i.e., ear, paw, and tail, observed at day 15 post Tamoxifen injectionand worsen over time by becoming visible throughout the entire skin from around one month post Tamoxifen injection (**Figure 4M**, **S4A**). The skin defect was associated with a thicker epidermis and higher proliferative activity in KO and HET compared to controls, as visualized by Ki67 immunostainings (**Figure 4A-D**, **S4B-E**). Moreover, dermal infiltration of immune cells, tortuous blood vessels, dilated lymphatic vessels, as well as enlarged inguinal and axillary lymph nodes, indicating high dynamics in lymphatic drainage, were observed in the dermis of KO and HET mice compared to control skin (**Figure 4E-L**). In contrast, these features were not observable at day 7 post Tamoxifen injection, except for the infiltration of Gr1-positive neutrophils, which appeared to be the first immune cells recruited to the dermis of KO and HET mice (**Figure 4N**, **S4F-H**). Together, these results pinpoint towards the hallmarks of a chronic inflammation-associated skin disease, suggesting that altered ATP6AP2 abundance leads to a defect in protein homeostasis associated with cellular stress and subsequent unresolved inflammation.

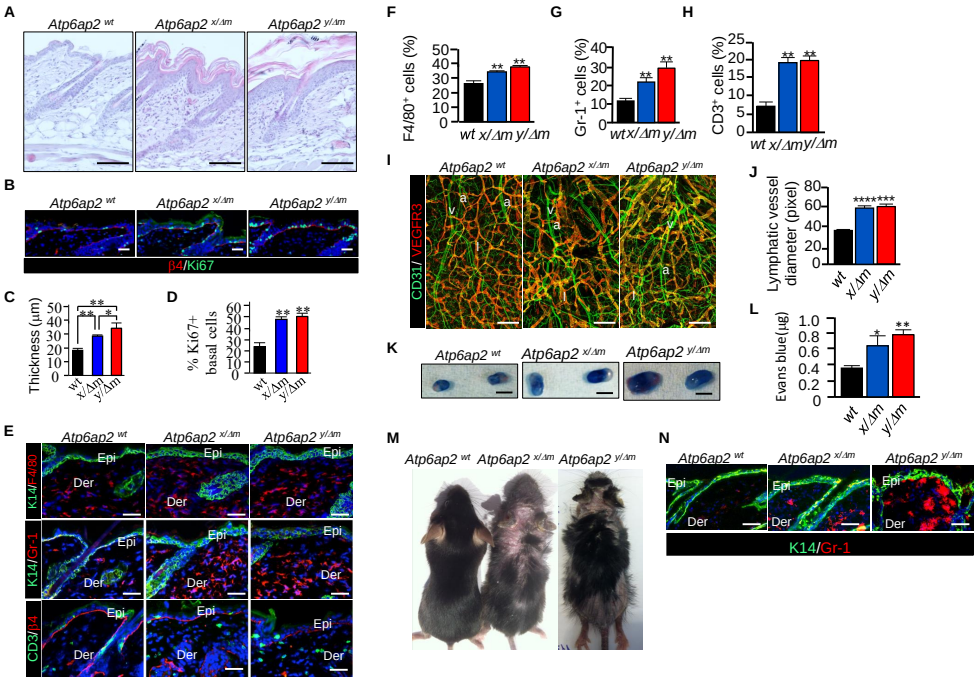

Figure 4 | Postnatal alteration of ATP6AP2 levels in the epidermis leads to chronic inflammation of the skin. (**A**) Hematoxylin and Eosin (H&E) staining of back skin sections from control, HET, and KO mice at day 15 post Tamoxifen injection. Scale bar: 50 μm. (**B**) Immunofluorescence labelling of sections through back skin isolated from control, HET, and KO mice at day 15 post Tamoxifen injection, with anti-β4 subunit integrin and anti-Ki67 antibodies. Scale bar: 20 μm. (**C**) Quantitative analysis of the thickness of the epidermis of back skin sections from control, HET, and KO mice at day 15 post Tamoxifen injection. (**D**) Quantitative analysis of the percentage of Ki67-positive cells in the epidermal basal layer of back skin sections from control, HET, and KO mice at day 15 post Tamoxifen injection. (**E**) Immunofluorescence labelling of sections through back skin isolated from control, HET, and KO mice at day 15 post Tamoxifen injection, with antibodies against Keratin 14 (K14) and F4/80 (upper panel), K14 and Gr-1 (middle panel), and CD3 and β4 subunit integrin (lower panel). Scale bar: 50 μm. (**F**) Quantitative analysis of F4/80-positive cells in the dermis of control, HET, and KO skin sections at day 15 post Tamoxifen injection. (**G**) Quantitative analysis of Gr1-positive cells in the dermis of control, HET, and KO skin sections at day 15 post Tamoxifen injection. (**H**) Quantitative analysis of CD3-positive cells in the dermis of control, HET, and KO skin sections at day 15 post Tamoxifen injection. (**I**) Whole-mount labeling of control, HET, and KO ear skin at day 15 post Tamoxifen injection with anti-CD31 and anti-VEGFR3 antibodies. Scale bar: 100 μm. (**J**) Quantitative analysis of the lymphatic vessel diameter in control, HET, and KO ear skin at day 15 post Tamoxifen injection. (**K**) Micrographs of inguinal lymph nodes isolated from control, HET, and KO skin sections at day 15 post Tamoxifen injection, after Evans blue intradermal injection. Scale bar: 250 mm. (**L**) Quantitative analysis of the Evans blue present in inguinal lymph node in control, HET, and KO mice at day 15 post Tamoxifen injection. (**M**) Micrographs of control, HET, and KO mice one month post Tamoxifen injection. (**N**) Immunofluorescence labelling of sections through back skin isolated from control, HET, and KO mice at day 7 post Tamoxifen injection, with antibodies against Keratin 14 (K14) and Gr-1. Scale bar: 50 μm.

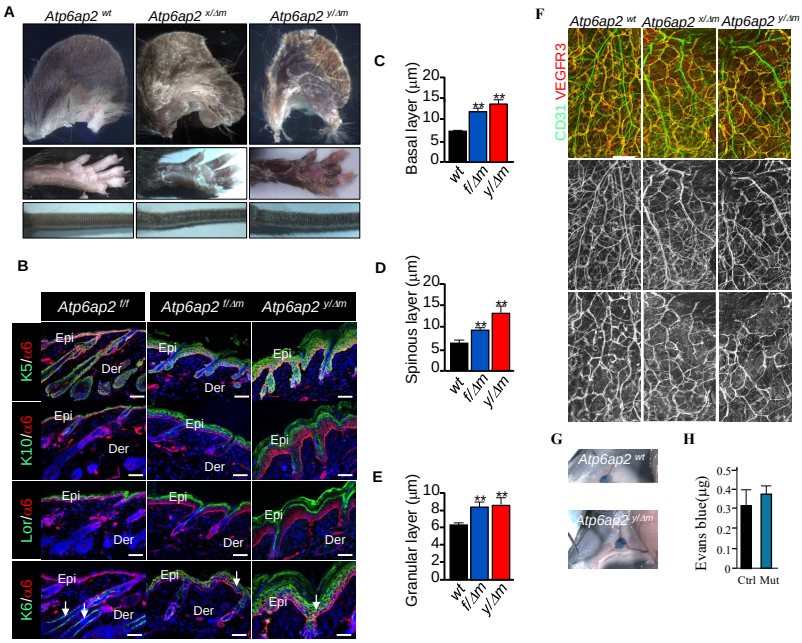

Figure S4 | (**A**) Micrograph of ear, paw, and tail from control, HET, and KO skin sections at day 15 post Tamoxifen injection. (**B**) Immunofluorescence labeling of back skin sections from control, HET, and KO skin sections at day 15 post Tamoxifen injection with antibodies against α6 subunit integrin and against markers of different layers of the epidermis, Keratin 5 (K5), Keratin 10 (K10), Loricrin (Lor), and Keratin 6 (K6). Scale bar: 50 μm. (**C**) Quantitative analysis of the thickness of the basal epidermis layer based on K5 labelling of back skin sections from control, HET, and KO at day 15 post Tamoxifen injection. (**D**) Quantitative analysis of the thickness of the spinous epidermis layer based on K10 labelling of back skin sections from control, HET, and KO at day 15 post Tamoxifen injection. (**E**) Quantitative analysis of the thickness of the granular epidermis layer based on Lor labelling of back skin sections from control, HET, and KO at day 15 post Tamoxifen injection. (**F**) Whole-mount labeling of control, HET, and KO ear skin at day 7 post Tamoxifen injection with anti-CD31 and anti-VEGFR3 antibodies. Scale bar: 100 μm. (**G**) Micrographs of inguinal lymph nodes of control, HET, and KO skin sections at day 7 post Tamoxifen injection, after Evans blue intradermal injection. (**H**) Quantitative analysis of the Evans blue present in inguinal lymph node in control and mutant mice at day 7 post Tamoxifen injection.

Supplementary Material

Mouse Strains

This study complied with French and Dutch government guidelines and directive 2010/63/EU of the European Parliament. All efforts were made to minimize the number of animals used and their suffering. The institutional Committees of Animal Welfare of Ile de France and Leiden University Medical Center (project numbers 2040.01 and AVD1160020171068; AVD1160020221609, respectively) approved all protocols. The mice carrying conditional *Atp6ap2* alleles (*Atp6ap2*$^{fl/fl}$) have been described elsewhere [9]. *K5-Cre* mice were kindly provided by Dr. J.L. Jorcano [23]. Rosa mT/mG (stock 007676) and Tg(KRT14-cre/ERT)20Efu/J (stock 005107) mouse strains were acquired from Jackson ImmunoResearch Laboratories. For all experiments, transgenic males expressing Cre recombinase were used in the mating. Cre; *Atp6ap2* $^{F/Y}$ knockout males and Cre; *Atp6ap2* $^{F/+}$ heterozygous females were compared to control litter mates (*Atp6ap2* $^{F/Y}$ males and *Atp6ap2* $^{F/F}$ females). For lineage-tracing experiments, E15.5 embryos of the *K5-Cre*/+; Rosa mT/mG/+ genotype were cryo-embedded, sectioned and analyzed by immunofluorescence. In this line, cells ubiquitously express the cell membrane-bound red fluorescent protein tdTomato (mT) under the control of the actin B promoter (ACTB), but in Cre recombinase expressing cells, mT is replaced by cell membrane-bound GFP (mG). Evaluation of lymphatic drainage was performed as described previously, with minor modifications [25]. In brief, mice were anesthetized and 1 µL g^{-1} of body weight solution of 3% Evans blue (Sigma) in PBS was injected subcutaneously in the lateral tail base, at 1 cm caudal to the rectum, and medial to the tail vein, using a Hamilton syringe. After 5 min, mice were sacrificed, and inguinal and axial lymph nodes were collected and incubated in 50 mL formamide (Fluka) at 55°C for 16 h. The extracted Evans blue was measured by absorbance at 620 nm and its concentration was calculated using a standard curve of Evans blue in formamide. Data were presented as absolute value of dye retained in left and right inguinal and axial lymph nodes. Convergence of blood and lymphatic vessels was accessed by injection of 1 µL of Tomato Lectin into the vitellin vein at E15.5. Back skin was isolated and stained with anti-VEGFR-3 antibody [26].

BrdU- or EdU-incorporation, Tissue Preparation, Whole-mount Staining, Histology, and Immunostaining

Mice were injected *intraperitoneally* with bromodeoxyuridine (BrdU), 1 mg g^{-1} of body weight, 1 h before tissue collection. Back or ear skins were either embedded in cryo-protectant (Tissue-Tek O.C.T.) or in paraffin and processed for sections (7 µm) or as whole-mount. Sections were used for Haematoxylin and Eosin (H&E) or immunofluorescence staining [27]. Whole-mount staining were performed as previously described [28]. Cells grown on glass coverslips were processed for immunostaining as previously described [27]. For EdU incorporation,

cells were incubated 3 h in presence of 10 mM EdU and subsequently stained using an EdU Click kit (BCK-EdU555, Sigma-Aldrich) according to the manufacturer's instructions. Cell nuclei were counter-stained with DAPI or Hoechst 33342. The antibodies used are listed in **Table 1**. Micrographs were acquired with Leica SP5 confocal, spinning disk, or Leica DM6000B microscopes.

Quantitative RT–PCR and RNA-Seq

RNA was isolated from back skin at E15.5 with the RNeasy kit (QIAGEN N.V., Hilden, Germany). Quantitative RT-PCR were performed as previously described [29]. The used primers are provided in **Table 2**. The values were normalized to glyceraldehyde phosphate dehydrogenase (*Gapdh*) expression levels using the comparative CT (ΔΔCT) method. RNA-Seq analysis was performed by Plateforme Génomique, Paris. In brief, library preparation was performed with Illumina TruSeq. Quality control on the reads was done with FastQC, high quality reads were aligned using STAR 2.6.1b, mapped reads were annotated using the reference genome mm10 (Ensembl version 96). Finally, sample expression was performed with HTSeq-count 0.9.1 (Eoulsan version). Next, we used DESeq 2 1.8.1r for gene expression normalization, subsequent differential expression testing and pathway analysis was performed in GSEA4.1.0 with (`http://download.baderlab.org/EM_Genesets/November_01_2019/Mouse/symbol/`) from the Bader Lab. R2 bioinformatics platform was used for analyzing and visualizing the data (`http://r2.amc.nl`).

Establishment of NMK-*Atp6ap2* $^{Flox/Y}$ Line, Viral Transduction, and Flow Cytometry

Normal mouse keratinocyte bearing *Atp6ap2* floxed allele (NMK-*Atp6ap2* $^{Flox/Y}$) were generated as described previously [27]. The adenoviral delivery of Cre recombinase or LacZ was performed with 5×10^{10} PFU mL^{-1} and 2.68×10^{10} PFU mL^{-1} viruses (SignaGen Laboratories, SL100707 and SL100714), respectively at MOI 100 for 24 h. For flow cytometry, cells were processed for single-cell suspension, incubated at 4°C for 1h with antibodies described in **Table 1**. Analysis was performed on LSRII flow-cytometer (Becton Dickinson).

Supplementary Tables

Table 1 | Antibody List.

Antibodies	Company	Reference number
α6 integrin	Thermo Fisher Scientific	GoH3 14-0495-82
β4 integrin	Abcam	ab25254
K14	BioLegend Covance	PRB-155P
K5	BioLegend Covance	PRB-160P
K6A	BioLegend Covance	PRB-169P
K10	BioLegend Covance	PRB-159P
Gr-1	eBioscience	RB6-8C5
CD3	FisherScientific	RM-9107-R7
CD31	BD Horizon	565509
VEGFR3	R&D Systems	BAF743
ATP6AP2	Covalab	This study, rabbit serum GLDELGKRYGEDSEQFRD
BrdU	Dako Cytomation	Clone Bu20a
Survivin	Cell Signaling	2808S
Loricrin	BioLegend Covance	PRB-145P
F4/80	Abcam	ab6640
Ki67	Abcam	ab15580

Table 2 | Primer List.

Primers	Company	Reference number
Gapdh	Qiagen	QT01658692
K14	Qiagen	QT00114422
Lor1	Qiagen	QT00248192
IL-33	Qiagen	QT00135170
K15	Qiagen	QT00122185
K10	Qiagen	QT00493241
Atp6ap2	5‘-CGGAAGTGCCAGTTTATCCA-3’	5‘-CTGTCCATGGGCTTCTCTGT-3’

References

[1] Nguyen G, Delarue F, Burcklé C, Bouzhir L, Giller T, Sraer JD. Pivotal role of the renin/prorenin receptor in angiotensin II production and cellular responses to renin. Journal of Clinical Investigation. 2002 Jun;109(11):1417-27.

[2] Nguyen G. Renin, (pro)renin and receptor: An update. Clinical Science (Lond). 2011 Mar;120(5):169-78.

[3] Cruciat Cm, Ohkawara B, Acebron SP, Karaulanov E, Reinhard C, Ingelfinger D, et al. Requirement of Prorenin Receptor. Science. 2010 Jan;327(5964):459-63.

[4] Buechling T, Bartscherer K, Ohkawara B, Chaudhary V, Spirohn K, Niehrs C, et al. Wnt/Frizzled signaling requires dPRR, the Drosophila homolog of the prorenin receptor. Current Biology. 2010 Jul;20(14):1263-8.

[5] Hermle T, Saltukoglu D, Grünewald J, Walz G, Simons M. Regulation of frizzled-dependent planar polarity signaling by a V-ATPase subunit. Current Biology. 2010 Jul;20(14):1269-76.

[6] Pamarthy S, Kulshrestha A, Katara GK, Beaman KD. The curious case of vacuolar ATPase: Regulation of signaling pathways. Molecular Cancer. 2018 Feb;17(1):41.

[7] Stransky L, Cotter K, Forgac M. The function of V-ATPases in cancer. Physiological Reviews. 2016 Jul;96(3):1071-91.

[8] Guida MC, Hermle T, Graham LA, Hauser V, Ryan M, Stevens TH, et al. ATP6AP2 functions as a V-ATPase assembly factor in the endoplasmic reticulum. Mol Biol Cell. 2018 Sep;29(18):2156-64.

[9] Riediger F, Quack I, Qadri F, Hartleben B, Park JK, Potthoff SA, et al. Prorenin receptor is essential for podocyte autophagy and survival. Journal of the American Society of Nephrology. 2011 Dec;22(12):2193-202.

[10] Oshima Y, Kinouchi K, Ichihara A, Sakoda M, Kurauchi-Mito A, Bokuda K, et al. Prorenin receptor is essential for normal podocyte structure and function. Journal of the American Society of Nephrology. 2011 Dec;22(12):2203-12.

[11] Song R, Preston G, Ichihara A, Yosypiv IV. Deletion of the Prorenin Receptor from the Ureteric Bud Causes Renal Hypodysplasia. PLoS ONE. 2013 May;8(5):e63835.

[12] Kinouchi K, Ichihara A, Sano M, Sun-Wada GH, Wada Y, Kurauchi-Mito A, et al. The (Pro)renin receptor/ATP6AP2 is essential for vacuolar H(+)-ATPase assembly in murine cardiomyocytes. Circulation Research. 2010 Jul;107(1):30-4.

[13] Kurauchi-Mito A, Ichihara A, Bokuda K, Sakoda M, Kinouchi K, Yaguchi T, et al. Significant roles of the (pro)renin receptor in integrity of vascular smooth muscle cells. Hypertension Research. 2014 Sep;37(9):830-5.

[14] Schafer ST, Han J, Pena M, Von Bohlen und Halbach O, Peters J, Gage FH. The Wnt adaptor protein ATP6AP2 regulates multiple stages of adult hippocampal neurogenesis. Journal of Neuroscience. 2015 Mar;35(12):4983-98.

[15] Dubos A, Castells-Nobau A, Meziane H, Oortveld MAW, Houbaert X, Iacono G, et al. Conditional depletion of intellectual disability and Parkinsonism candidate gene ATP6AP2 in fly and mouse induces cognitive impairment and neurodegeneration. Human molecular genetics. 2015 Dec;24(23):6736-55.

[16] Ramser J, Abidi FE, Burckle CA, Lenski C, Toriello H, Wen G, et al. A unique exonic splice enhancer

mutation in a family with X-linked mental retardation and epilepsy points to a novel role of the renin receptor. Human Molecular Genetics. 2005 Apr;14(8):1019-27.

[17] Poorkaj P, Raskind WH, Leverenz JB, Matsushita M, Zabetian CP, Samii A, et al. A novel X-linked four-repeat tauopathy with Parkinsonism and spasticity. Movement Disorders. 2010 Jul;25(10):1409-17.

[18] Hirose T, Cabrera-Socorro A, Chitayat D, Lemonnier T, Féraud O, Cifuentes-Diaz C, et al. ATP6AP2 variant impairs CNS development and neuronal survival to cause fulminant neurodegeneration. Journal of Clinical Investigation. 2019 Apr;129(5):2145-62.

[19] Rujano MA, Serio MC, Panasyuk G, Péanne R, Reunert J, Rymen D, et al. Mutations in the X-linked ATP6AP2 cause a glycosylation disorder with autophagic defects. Journal of Experimental Medicine. 2017 Dec;214(12):3707-29.

[20] Cannata Serio M, Rujano MA, Simons M. Mutations in ATP6AP2 cause autophagic liver disease in humans. Autophagy. 2018;14(6):1088-9.

[21] Jansen EJR, Timal S, Ryan M, Ashikov A, Van Scherpenzeel M, Graham LA, et al. ATP6AP1 deficiency causes an immunodeficiency with hepatopathy, cognitive impairment and abnormal protein glycosylation. Nature Communications. 2016 May;7:11600.

[22] Raymond K, Martin S, Aractingi S, Lebrin F. The (pro)renin receptor controls Wnt signalling: promise from Drosophila and Xenopus. European journal of dermatology. 2013 Apr.

[23] Ramirez A, Page A, Gandarillas A, Zanet J, Pibre S, Vidal M, et al. A keratin K5Cre transgenic line appropriate for tissue-specific or generalized Cre-mediated recombination. Genesis. 2004 May;39(1):52-7.

[24] Vasioukhin V, Degenstein L, Wise B, Fuchs E. The magical touch: Genome targeting in epidermal stem cells induced by tamoxifen application to mouse skin. Proceedings of the National Academy of Sciences of the United States of America. 1999 Jul;96(15):8551-6.

[25] Harrell MI, Iritani BM, Ruddell A. Lymph node mapping in the mouse. Journal of Immunological Methods. 2008 Mar;332(1-2):170-4.

[26] Böhmer R, Neuhaus B, Bühren S, Zhang D, Stehling M, Böck B, et al. Regulation of Developmental Lymphangiogenesis by Syk+ Leukocytes. Developmental Cell. 2010 Mar;18(3):437-49.

[27] Raymond K, Kreft M, Janssen H, Calafat J, Sonnenberg A. Keratinocytes display normal proliferation, survival and differentiation in conditional β4-integrin knockout mice. Journal of Cell Science. 2005 Mar;118(Pt 5):1045-60.

[28] Lebrin F, Srun S, Raymond K, Martin S, Van Den Brink S, Freitas C, et al. Thalidomide stimulates vessel maturation and reduces epistaxis in individuals with hereditary hemorrhagic telangiectasia. Nature Medicine. 2010 Apr;16(4):420-8.

[29] Thalgott JH, Dos-Santos-Luis D, Hosman AE, Martin S, Lamandé N, Bracquart D, et al. Decreased expression of vascular endothelial growth factor receptor 1 contributes to the pathogenesis of hereditary hemorrhagic telangiectasia type 2. Circulation. 2018 Dec;138(23):2698-712.

Disclosure Statement: All authors declare no competing interests.

Funding: This work was supported by the Agence Nationale de la Recherche ANR_grant SVSE-2_Epi-PRR lymph. K. Raymond and F. Lebrin are chargé de Recherche at the Insitut National de la Santé et de la Recherche Médicale (INSERM).

Acknowledgments: We are particularly grateful to Dr. J.L. Jorcano from the Department of Bioengineering, Carlos III University, Madrid, Spain for providing *K5-Cre* transgenic mice.